Liquid Crystals

In Situ Synthesis and Assembly of Gold Nanoparticles Embedded in Glass-Forming Liquid Crystals**

V. Ajay Mallia, Praveen Kumar Vemula, George John, Ashavani Kumar, and
Pulickel M. Ajayan**

It is of tremendous interest to use nanoparticles (NPs) as building blocks for the fabrication of multifunctional meso-scale assemblies by organizing them into two- and three-dimensional structures with precise size and shape control for applications based on their collective properties.[1,2] Several ways have been reported to create ordered assemblies of NPs by using templates that have sites with specific binding to NPs,[3] for example, self-assembled monolayers,[4] surface-modified polymers,[5] electrophoretic assembly onto suitable substrates,[6] electrostatic attachment to Langmuir monolayers at the air–water interface[7–10] and air–organic solvent interface, hydrogels,[11] and by diffusion into ionizable fatty lipid films,[12] DNA,[13–15] and so on. However, in those instances the synthesis and assembly of NPs are done in multiple steps. Therefore, it would be extremely useful if one could develop a protocol in which the templates used for the assembly can also provide active sites for reducing the nanoparticle precursors so that the formation and assembly of the nanoparticles are achieved in one single step.

An ideal candidate template for NP assembly would be liquid crystal (LC) materials that have direct function in display applications, ferroelectric materials, and photonics, among others, and could be tailored/tuned easily in any two- or three-dimensional structures by using external stimuli such as light and electric or magnetic fields. LCs are self-organizing materials characterized by their uniaxial, lamellar, helical, or columnar arrangement in nematic, smectic, cholesteric, and discotic phases, respectively.[16] With their molecular arrange-

ments frozen, glassy LCs (GLCs) represent a class of materials that combine properties intrinsic to LCs with those common to polymers. The advantage of GLCs is that they can be processed like conventional LCs but maintain their optical property and molecular alignment when cooled into a solid phase.[17] Thus, GLCs would be suitable hosts for synthesizing and aligning the NPs.

LC-embedded metal nanoparticles (MNPs) and inorganic porous networks have been studied in recent years.[18–25] However, most of these processes involve multiple steps that involve separate synthesis of metal nanoparticles, their functionalization, and doping of particles in LC domains. Another major problem is destabilization of LC domains during incorporation of MNPs owing to chemisorption of LC mesogens on the NPs.[21] Hence, we reasoned that the development is necessary of a suitable procedure in situ to generate GLC–MNP conjugates whereby chemisorption is reduced and where well-aligned NP arrays produce novel hybrid materials.

Herein, we demonstrate a novel approach to obtain the MNPs embedded in LCs based on the synthesis in situ of MNPs by using glass-forming mesogens without any external reducing and stabilizing agents. New low-molecular-weight mesogens were synthesized that could reduce metal salts to nanoparticles as well as form glassy LC phases. These thermotropic liquid-crystalline systems were used for synthesis in situ and spontaneous assembly of MNPs in LC phases into mesostructures. We also successfully demonstrate to some extent the ability to control shapes of NPs obtained in different LC phases owing to the templating effect of the inherent LC domains. The major advantage of this approach is that we could achieve assembly of MNPs directly from metal ions without a separate synthesis of MNPs and their later derivatization. In the present case, MNPs embedded in LCs were highly stable and showed LC properties at room temperature.

We synthesized new amphiphilic low-molecular-weight mesogens, **A11**, **A7**, and **A5**, containing cholesterol (mesogenic core) and aniline (known to reduce HAuCl₄[26,27]) groups with different methylene chains (Scheme 1). A detailed synthetic scheme of amphiphiles is discussed in the Supporting Information. The LC properties of newly synthesized mesogens (e.g. **A11** to **A5**) were examined using a polarized optical microscope (POM) and differential scanning calorimetry (DSC) studies (Figures 1 and 2, respectively).

Mesogen **A5** melts to a chiral smectic A (SmA*) phase at 67.9 °C before changing into an isotropic phase at 79.8 °C. The SmA* phase was identified from its characteristic homeo-

[*] Dr. V. A. Mallia,[+] Dr. P. K. Vemula,[+] Prof. G. John
Department of Chemistry
The City College and the City University of New York
New York, New York 10031 (USA)
Fax: (+1) 212-650-6107
E-mail: john@sci.ccny.cuny.edu
Homepage: http://www.sci.ccny.cuny.edu/chemistry/faculty/
john.html

Dr. A. Kumar, Prof. P. M. Ajayan
Department of Material Science and Engineering
Rensselaer Polytechnic Institute
Troy, New York 12180 (USA)
Fax: (+1) 518-276-8554
E-mail: ajayan@rpi.edu
Homepage: http://www.rpi.edu/dept/materials/PMA/

[+] These authors contributed equally to this work.
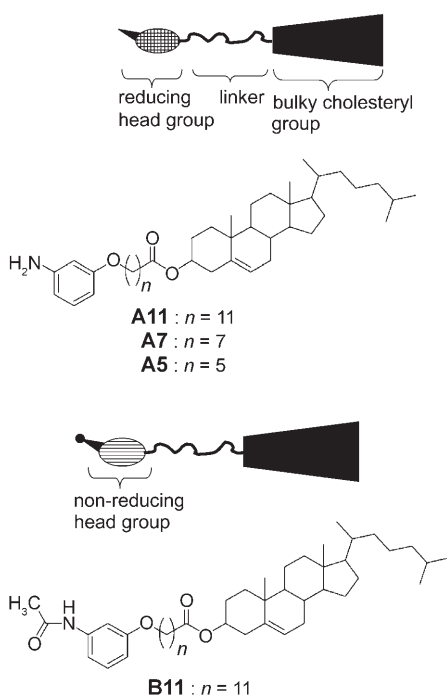
Scheme 1. Chemical structures of both types of amphiphiles containing reducing (amine) and non-reducing (amide) groups connected to cholesteryl mesogens.
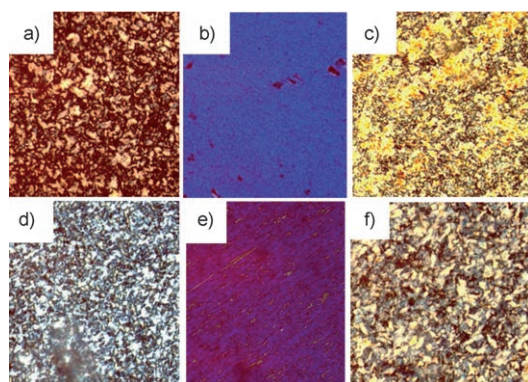

Figure 1. Polarized optical micrographs of a) SmC* (40.2°C, cooling cycle), b) N* (51.1°C, cooling cycle), and c) glassy phases of **A11**. POM images of LC phases formed by **A11**–GNP conjugates (prepared using 0.7 mol% gold chloride solution) of d) SmC* (42.2°C, cooling cycle), e) N* (51.7°C, cooling cycle), and f) glassy phases.

angle peaks corresponding to the interlayer spacings (*d*) at 64.1 and 37.2 Å accompanied by a diffuse peak at higher angles (5.1 Å). The molecular length of **A11** determined from a molecular model in the extended conformation by using the molecular mechanics 2 (MM2) method was found to be 39.8 Å. Interlayer distances observed in **A11** may represent tilted bilayer (64.1 Å) and tilted monolayer (37.2 Å) arrangements. Coexistence of multiple periodicities has been reported in the literature for dimeric liquid crystals[29] and predicted for polar molecules.[30] The smaller *d* spacing values (for the bilayer and monolayer) in conjunction with striped focal conic textures and Schlieren textures observed in **A11** confirms the formation of a SmC* phase. More detailed investigation on interlayer spacings (*d*) and other optical properties of these molecules are in progress. Thermal properties of **A11** to **A5** are described in Table 1. With such

Table 1: Phase-transition temperatures and enthalpies of investigated mesogens.

		Phase-transition temperature [°C][a,b] (ΔH [kJ mol^{-1}])[c]		
A5	heating	Cr 67.9(14.7) SmA* 79.8(2.7) Iso		
	cooling	Iso 78.5(2.7) SmA* −6.3(0.7) G		
A7	heating	Cr 68.6(16.8) SmA* 73.0 TGBA* N* 77.5(0.13) Iso		
	cooling	Iso 76.5(0.6) N* 68.7 TGBA* 68.2 SmA* −2.0(0.8) G		
A11	heating	Cr 38.7(12.8) SmC* 45.1(0.6) N* 68.3(1.0) Iso		
	cooling	Iso 66.9(0.6) N* 43.1(0.5) SmC* 6.0(0.4) G		
B11	heating	Cr 105.5 Iso		
	cooling	Iso 85.9 Cr		

[a] Transition temperatures were obtained from DSC analysis at a rate of 5°C min^{-1}. [b] Cr = crystalline, SmA* = chiral smectic A, TGBA* = twist grain boundary phase, SmC* = chiral smectic C phase, N* = chiral nematic, Iso = isotropic, and G = glassy phase. [c] ΔH values are given in parentheses.

intriguing LC systems, we explored their ability in gold nanoparticle (GNP) synthesis by reduction in situ to produce GNPs embedded in LCs as hybrid materials. Typically, a homogeneous solution of mesogen and HAuCl$_4$ (0.7–5 mol%) in acetone was drop-casted on a glass plate and the solvent was evaporated to form a light-yellow film (Figure 2a). The film thus obtained was heated at 100°C for 60 s and cooled to room temperature. On heating, the yellow film rapidly turned colorless and then pale pink (see Figure 2a and the Supporting Information). It is proposed that these changes are consistent with the initial rapid reduction of Au^{III} to Au^I followed by reduction of Au^I to Au^0.[11] The UV/ Vis spectra of LC films as a function of the gold chloride concentration used for the preparation of the GNPs are shown in Figure 2b. The black, red, and green curves show the absorption spectra of the NPs prepared using **A11** and 0.7, 2.5, and 5 mol% gold chloride, respectively. All three curves show a characteristic absorbance at 573 nm, which corresponds to the surface-plasmon band of the GNPs. The absorption intensity of the film increased upon increasing the gold chloride concentration with no shift in the surface-plasmon resonance. The optical properties of GNP–LCs do not change with time, indicating that the particles are stable in the LC matrix without showing phase separation.

tropic and focal conic textures that were observed by using a POM.[28] Interestingly, upon cooling, SmA* transformed into a glassy LC phase. Similarly mesogen **A7** formed an SmA* phase at 68.6°C and it also exhibited a twist grain boundary phase (TGBA*).[28] During slow heating, the filament structure of the TGBA* phase grows slowly into the homeotropic regions of the SmA* phase and subsequently turns into a chiral nematic (N*) phase.[28] Mesogen **A11** melted to a SmC* phase, which was confirmed from its broken fan-shaped texture with dechiralization lines.[28] Small-angle X-ray measurements at 40°C (cooling cycle) of **A11** showed sharp lower-

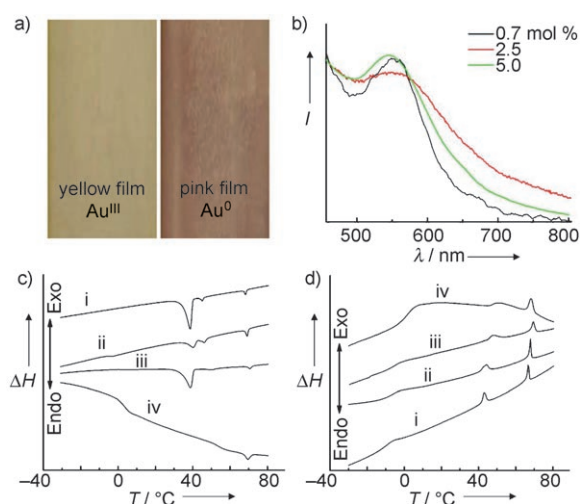© 2007 Wiley-VCH Verlag GmbH & Co. KGaA, Weinheim

Figure 2. a) Glass plates coated with **A11** and HAuCl$_4$ at 25 °C, before heating (yellow; left) and after heating at 100 °C followed by slow cooling to 25 °C (pink; right). b) Absorption spectra obtained for the **A11** glassy LC films containing gold nanoparticles prepared with different concentration of HAuCl$_4$ (I = intensity). DSC thermograms obtained from the third cycle of heating (c) and cooling cycles (d) from **A11** with difference amounts of HAuCl$_4$: i) 0, ii) 0.7, iii) 2.5, and iv) 5 mol% (ΔH = heat (enthalpy) change).

Figure 3. a) Schematic diagram of hypothetical LC-template-assisted alignment of GNP arrays. b) TEM image of the SmC* domain from **A11**. c–f) TEM images of GNPs embedded in SmC* domains of **A11** with low and high magnifications. Scale bars: 200 nm. In all cases, HAuCl$_4$ (5 mol% **A11**) was used for GNP synthesis.

To investigate the effect of inclusion of GNPs in LC systems, we studied the LC properties of **A11**–GNP conjugates. POM images of various LC phases formed by **A11** with and without GNPs are shown in Figure 1. Furthermore, we determined phase-transition temperatures by DSC, which gave insights into the thermal stability of these hybrid materials. Figure 2 c,d shows DSC thermograms obtained for GNPs embedded in **A11** LCs that were prepared by using different mol% values of HAuCl$_4$.

The higher melting temperatures of **A11**–GNP conjugates compared with **A11** alone indicate the stabilization of the LC phase by the GNPs. Intriguingly, an increase of about 11 °C in the LC glass-transition temperature was observed in **A11**–GNPs that were prepared by using 5 mol% of HAuCl$_4$, compared with **A11** alone (Figure 2 d). Earlier studies[20] showed that physical mixtures of LC–NP hybrid systems lower the glass-transition temperatures (destabilization) of LC phases by the MNPs owing to the chemisorption of mesogens on NPs. However, in the present study, GNPs were generated in situ by using mesogens as reducing and stabilizing agents, thus, there would be no further chemisorption expected and the LC phases may be stabilized.

To examine the various organizations of GNPs in the LC matrix, similar experiments were carried out on a carbon-coated grid and silicon wafer for transmission electron microscopy (TEM) and scanning electron microscopy (SEM), respectively, with and without HAuCl$_4$. Figure 3 b,c shows the TEM images of the mesogen **A11** domain without and with GNPs, respectively. Both images show the domains of the twisted-ribbon morphology with a width of approximately 120–140 nm and length of approximately 1–2 μm (Figure 3 b,c; see also Figure S3 in the Supporting Information). These domains are uniformly distributed all over the
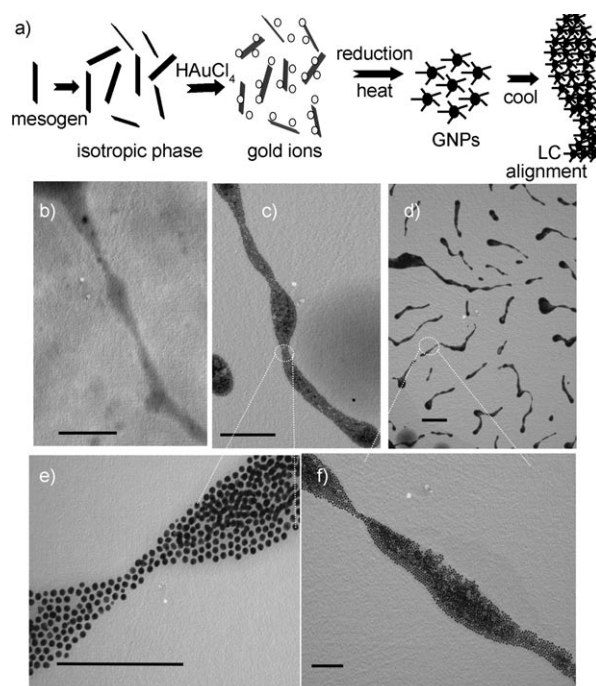
grid as shown in Figure 3 d. Figure 3 e,f show the higher-magnification images obtained from Figure 3 c,d and indicate that these domains are composed of close-packed GNPs with a size range of about 10–12 nm and an interparticle distance of approximately 2–4 nm. Notably, all NPs were distributed inside the LC domains, which was further confirmed by examination under SEM (see Figure S2 in the Supporting Information). The mechanism of confinement of gold nanoparticles is fairly well understood. We believe that gold ions first become entrapped in the LC domains owing to electrostatic complexation between AuCl$_4^-$ and the NH$_3^+$ group[26] of the mesogens and that their subsequent reduction results in nanoparticle formation in a well-defined 3D structure. Aromatic amines are known to reduce gold ions as well as stabilize the GNPs,[26,27] and aniline-modified LCs also behave in this way. Furthermore, in the present case, GNPs prepared in situ interacted with the terminal amines of highly oriented LC molecules and were then organized within the LC domains. When the GNPs embedded in glassy LC films were dissolved in acetone and observed with TEM, no regular pattern of the GNPs was seen (Figure 4 c). This suggests the role of LC phases in organizing the GNPs. Aging of the sample did not change the morphologies of the LC phase, which retained the patterned arrays for several months, and therefore indicates that the particles are stabilized with LC molecules and that they do not disturb the LC phases over a long period of time.

As this method involves LC domains that act as stabilizing agents, reducing agents, and templates for the formation of
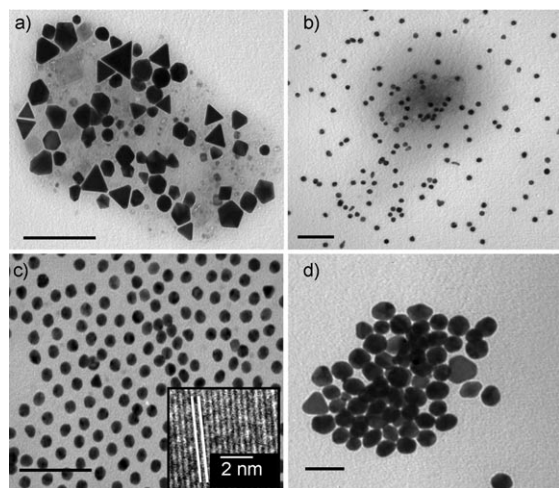
Figure 4. TEM images of GNPs prepared at the isotropic phase (100°C) of **A11** with different amounts of $HAuCl_4$: a) 0.7, b) 2.5, and c) 5 mol%. d) GNPs prepared in $CHCl_3$ solution using 5 mol% gold salt. Scale bars: 50 nm. The inset of (c) shows a high-resolution TEM image of a multiply twinned Au nanoparticle and lattice planes.

Figure 5. TEM images of GNPs prepared in different LC phases (5 mol% of $HAuCl_4$ used). a) SmC*, b) N*, and c) isotropic phases of **A11**; and d) SmA* phase of **A5** in the supercooled state (arrows indicate helical morphology). Scale bars: 50 nm.

nanoparticles, the next logical step will be to explore the possibility of controlling the shape and size of nanoparticles. This could be done either by polymorphic LC transitions of the mesogens to vary the microstructure of the LC domains or through varying the concentration of gold chloride used for the synthesis of GNPs.

Initially we studied the effect of gold concentration on GNP properties in the isotropic phase followed by the effect of LC phases on the size and shape of GNPs. First, the reduction process was carried out with various amounts of $HAuCl_4$ (0.7, 2.5, and 5 mol%) in an isotropic phase to produce different sizes and shapes of GNPs. LC–GNP hybrid systems prepared by using 0.7 mol% of $HAuCl_4$ exhibited different shapes of GNPs such as platelike, pyramids (cross section: triangles), cubes (squares), dodecahedra (pentagons, hexagons), and spheres (circular) with sizes ranging from 12 to 35 nm (Figure 4a). In contrast, the LC–GNPs prepared with 2.5 and 5 mol% of $HAuCl_4$ form uniform spherical particles with average sizes of (16 ± 2) nm and (14 ± 2) nm, respectively (Figure 4b,c). The inset of Figure 4c shows the high-resolution TEM image of the nanoparticles acquired by using a Jeol 200 kV TEM. The lattice spacing observed in the GNP (corresponding to a multiply twinned particle, commonly observed in gold particles) of 2.39 Å corresponds to Au (111) planes. The size distributions obtained in several cases correspond to a Gaussian distribution (see Figure S4 in the Supporting Information).

To investigate the influence of molecular ordering of LCs on the growth of NPs, we prepared GNPs by using 5 mol% of $HAuCl_4$ in different LC phases formed by **A11**, **A7**, and **A5**. As indicated earlier, **A11** exhibits the SmC* phase from 38.7°C, which then transforms to a N* phase at 45.1°C, hence, we prepared GNPs at the SmC* (40°C), N* (55°C), and isotropic phases (100°C). For GNPs formed in different LC phases, samples were placed at the above-mentioned temperatures and heated at the SmC* and N* phases. Interestingly,
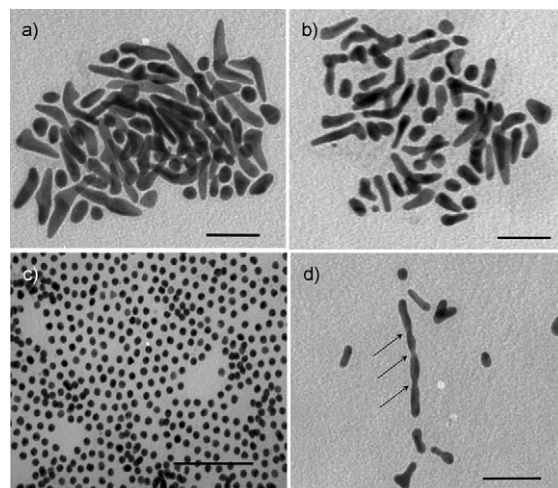
we observed a dramatic change in size and shape (morphology) of the GNPs in the presence of LC phases. TEM images show that GNPs prepared in different LC phases exhibit different morphologies (Figure 5). GNPs prepared in SmC* were shaped as boomerangs and displayed irregular rodlike morphologies (Figure 5a); spheres were also observed for GNPs prepared in the N* phase (Figure 5b). Typical lengths of the rods were 20–23 nm with widths of 8–10 nm. In the case of GNPs prepared in the isotropic phase, monodispersed well-separated spherical NPs were observed with sizes of (14 ± 2) nm (Figure 5c). More promisingly, GNPs prepared in the SmA* phase of **A5** showed occasional helical morphology (Figure 5d; 120–140 nm in length and 10–12 nm in width). These results suggest that LC phases influence the size and morphology of the GNPs prepared in situ. It may be suggested that the positional or molecular orientation of highly ordered LC phases directs the NPs growth and subsequently controls the morphologies of the GNPs formed in situ. A hypothetical scheme for the formation of different shapes of NPs is given in the Supporting Information). The presence of NPs with different shapes suggests that shape selectivity was not completely achieved, however, this positive indication would signify the possible appreciable shape-selective synthesis of NPs by using precisely designed LC mesogens. Further experiments are in progress to improve the shape selectivity of the nanoparticles.

To explore the importance of the amine group in the gold reduction process, we synthesized amphiphile **B11** (Scheme 1), which has a similar structure to **A11** with the exception of a terminal acetanilide group. Compound **B11** failed to show LC behavior or reduce the gold to produce GNPs under similar conditions as were used in **A11**-mediated GNP synthesis. This highlights the importance of the free terminal amine group in GNP formation. ^{1}H NMR spectroscopic studies carried out to gain insight into the binding of amine group to the gold (see the Supporting Information)

showed that the peak corresponding to the amine protons significantly broadens after the HAuCl₄ reduction when compared with **A11**. This suggests that after reduction the amine group binds to the gold to stabilize the NPs.[11]

In conclusion, we have reported, for the first time, the shape-selective synthesis of GNPs in glass-forming liquid-crystalline materials in a single step without using any external reducing and stabilizing agents. The inclusion of GNPs in LCs did not change the inherent LC properties and the LC phases were thermally stabilized. The size and shape of the GNPs depends on the relative amount of the gold chloride used and the LC phase. Unique morphology of the GNPs was achieved by tuning the concentration of the gold and selecting the different LC phases. In this in situ synthetic approach, all the GNPs are self-assembled within the LC domains and the entire process (formation and assembly) occurs in a single step, revealing ordered hierarchies at multiple length scales (nano to micro). We are exploring the utility of stable LC–GNP hybrid materials in the development of wide-angle LC displays. We envisage that the present approach could have applications in developing feasible methods for the generation of organic–inorganic hybrid materials, which can find potential use in advanced display devices.

Experimental Section

All reagents and solvents were purchased from Acros Chemicals (Fisher Scientific Company, Suwane, GA) and used without purification unless otherwise mentioned. The high-resolution proton NMR spectra of all the intermediates and the compounds were recorded on a Varian (300 MHz) spectrometer using CDCl₃ as solvent.

Characterization of LCs: Phase transitions were observed by using a polarized optical microscope (Leica DMLB2) equipped with a hot stage (Mettler, FP82) and a heating/cooling rate of 5 K min⁻¹. Further DSC studies were performed by using a Mettler DSC-822 equipped with a nitrogen-gas intracooling system. The thermograms were recorded at a heating rate of 5 °C min⁻¹. Samples were placed in an aluminum pan and sealed. An empty sealed aluminum pan was used as a reference cell. For the DSC studies of GNP-containing mesogens, a homogeneous solution of mesogen and HAuCl₄ (0.7–5 mol %) in acetone was drop-cast on a glass plate and the solvent was evaporated. The glass plate was heated to reach the isotropic phase where GNPs were generated, and the GNPs encapsulated by mesogens were transferred into the DSC pan for the measurements. X-ray diffraction (XRD) was performed on a Rigaku R-AXIS image plate system with Cu$_{K\alpha}$ X-rays ($\lambda = 1.540$ Å) generated with a Rigaku generator operating at 46 kV and 40 mA.

Preparation of GNPs and characterization: A homogeneous solution of mesogen and HAuCl₄ (0.7–5 mol %) in acetone was drop-cast onto a glass plate, and the solvent was evaporated to form a light-yellow film. The film thus obtained was heated to different temperatures (corresponding to the phase-transition temperatures of various LC phases) on the hot stage, the temperature was kept constant for 3–5 min, and the sample was then cooled to room temperature. At room temperature, stable glassy LC films were obtained.

UV/Vis spectroscopy: UV/Vis spectra of the GNPs embedded in LCs in the glassy films and solution phases were recorded on a CARY100BIO spectrophotometer. A UV/Vis spectrum was recorded by two methods. First, the obtained GNPs embedded in glassy films on typical laboratory glass slide were directly inserted into the UV/Vis spectrophotometer and recorded while keeping a plain glass slide as the reference. Alternatively, after preparation, the glassy films

were dissolved in a minimum amount of appropriate solvent and the absorption was acquired in a quartz cuvette with a path length of 1 cm.

TEM studies: TEM spectra were recorded by using a Zeiss EM 902 transmission electron microscope (80 kV). TEM experiments were performed by two methods. First, GNPs embedded in glassy LC films (SmC*, N*, and SmA*) were dissolved in a minimum amount of acetone and a drop was placed on a Cu grid. After drying at ambient conditions, the drop was examined under the electron microscope. Second, for alignment experiments, a homogeneous solution of mesogen and HAuCl₄ in acetone was drop-cast on a Cu grid. After drying the grid at ambient temperature, it was then placed on a hot stage and heated to 100 °C to obtain an isotropic phase. This was followed by slow cooling to room temperature. GNPs embedded in an aligned glassy LC film were obtained on a Cu grid and the grid was then directly examined under the electron microscope. Lattice resolution images of the nanoparticles were obtained in a JEOL 2010 instrument operated at 200 kV.

SEM studies: A homogeneous solution of mesogen and HAuCl₄ in acetone was drop-cast on a silicon wafer. After drying the silicon wafer at ambient temperature, it was placed on a hot stage and heated to 100 °C to obtain an isotropic phase. This was followed by slow cooling to room temperature. An aligned glassy LC film with embedded GNPs was obtained on the silicon wafer, which was directly examined under a field emission scanning electron microscope (JEOL 6330F FESEM) operated at 5 kV.

[1] M. P. Pileni, *J. Phys. Chem. B* **2001**, *105*, 3358–3371.
[2] C. Joachim, J. K. Gimzewski, A. Aviram, *Nature* **2000**, *408*, 541–548.
[3] M.-C. Daniel, D. Astruc, *Chem. Rev.* **2004**, *104*, 293–346.
[4] I. W. Hamley, *Angew. Chem.* **2003**, *115*, 1730–1752; *Angew. Chem. Int. Ed.* **2003**, *42*, 1692–1712.
[5] M. Möller, J. P. Spatz, A. Roescher, *Adv. Mater.* **1996**, *8*, 337–340.
[6] J. C. Loudet, P. Barois, P. Paulin, *Nature* **2000**, *407*, 611–613.
[7] P. Paulin, H. Stark, T. C. Lubensky, D. A. Weitz, *Science* **1997**, *275*, 1770–1773.
[8] I. Gascon, J.-D. Marty, T. Gharsa, C. Mingotaud, *Chem. Mater.* **2005**, *17*, 5228–5230.
[9] S. P. Meeker, W. C. K. Poon, J. Crain, E. M. Terentjev, *Phys. Rev. E* **2000**, *61*, R6083–R6086.
[10] R. Jin, Y. Cao, C. A. Mirkin, K. L. Kelly, G. C. Schatz, J. G. Zheng, *Science* **2001**, *294*, 1901–1903.
[11] P. K. Vemula, G. John, *Chem. Commun.* **2006**, 2218–2220.
[12] N. Kimizuka, T. Kunitake, *Adv. Mater.* **1996**, *8*, 89–91.
[13] G. P. Mitchell, C. A. Mirkin, R. L. Letsinger, *J. Am. Chem. Soc.* **1999**, *121*, 8122–8123.
[14] C. A. Mirkin, R. L. Letsinger, R. C. Mucic, J. J. Storhoff, *Nature* **1996**, *382*, 607–609.
[15] a) A. P. Alivisatos, K. P. Johnsson, X. Peng, T. E. Wilson, C. J. Loweth, Jr., M. P. Bruchez, P. G. Schultz, *Nature* **1996**, *382*, 609–611; b) J. Zheng, P. E. Constantinou, C. Micheel, A. P. Alivisatos, R. A. Kiehl, N. C. Seeman, *Nano Lett.* **2006**, *6*, 1502–1504.
[16] *Handbook of Liquid Crystal Research* (Eds.: P. J. Collings, J. S. Patel), Oxford University Press, New York, **1997**.
[17] V. A. Mallia, N. Tamaoki, *Chem. Soc. Rev.* **2004**, *33*, 76–84.

[18] a) K. Robbie, D. J. Broer, M. J. Brett, *Nature* **1999**, *399*, 764–766; b) *Liquid Crystals in Complex Geometries* (Eds.: G. P. Crawford, S. Zumer), Taylor and Francis, London, **1996**.

[19] L. Dolgov, O. Yaroschehuk, *Mol. Cryst. Liq. Cryst.* **2004**, *409*, 77–89.

[20] M. Mitov, C. Portet, C. Bourgerette, E. Snoeck, M. Verelst, *Nat. Mater.* **2002**, *1*, 229–231.

[21] B. V. Barmatov, D. A. Pebalk, M. V. Barmatova, *Langmuir* **2004**, *20*, 10868–10871.

[22] a) C. DaCruz, O. Sandre, V. Cabuil, *J. Phys. Chem. B* **2005**, *109*, 14292–14299; b) N. Kanayama, O. Tsutsumi, A. Kanazawa, T. Ikeda, *Chem. Commun.* **2001**, 2640–2641; c) I. In, Y.-W. Jun, Y. J. Kim, S. Y. Kim, *Chem. Commun.* **2005**, 800–801; d) M. Yamada, Z. Shen, M. Miyake, *Chem. Commun.* **2006**, 2569–2571; e) W. Dobbs, J.-M. Suisse, L. Douce, R. Welcher, *Angew.*

Chem. **2006**, *118*, 4285–4288; *Angew. Chem. Int. Ed.* **2006**, *45*, 4179–4182.

[23] L. Qi, Y. Gao, J. Ma, *Colloids Surf. A* **1999**, *157*, 285–294.

[24] L. Cseh, G. H. Mehl, *J. Am. Chem. Soc.* **2006**, *128*, 13376–13377.

[25] H. Qi, T. Hegmann, *J. Mater. Chem.* **2006**, *16*, 4197–4205.

[26] C. Subramaniam, R. T. Tom, T. Pradeep, *J. Nanopart. Res.* **2005**, *7*, 209–217.

[27] P. R. Selvakannan, P. S. Kumar, A. S. More, R. D. Shingte, P. P. Wadgaonkar, M. Sastry, *Adv. Mater.* **2004**, *16*, 966–971.

[28] I. Dierking, *Texture of Liquid Crystals*, Wiley-VCH, Weinheim, **2003**.

[29] a) V. A. Mallia, N. Tamaoki, *Chem. Commun.* **2004**, 2538–2539; b) D. W. Lee, J.-I. Jin, M. Laguerre, M. F. Achard, F. Hardouin, *Liq. Cryst.* **2000**, *27*, 145–152.

[30] J. Prost, P. Barois, *J. Chim. Phys.* **1983**, *80*, 65–81.